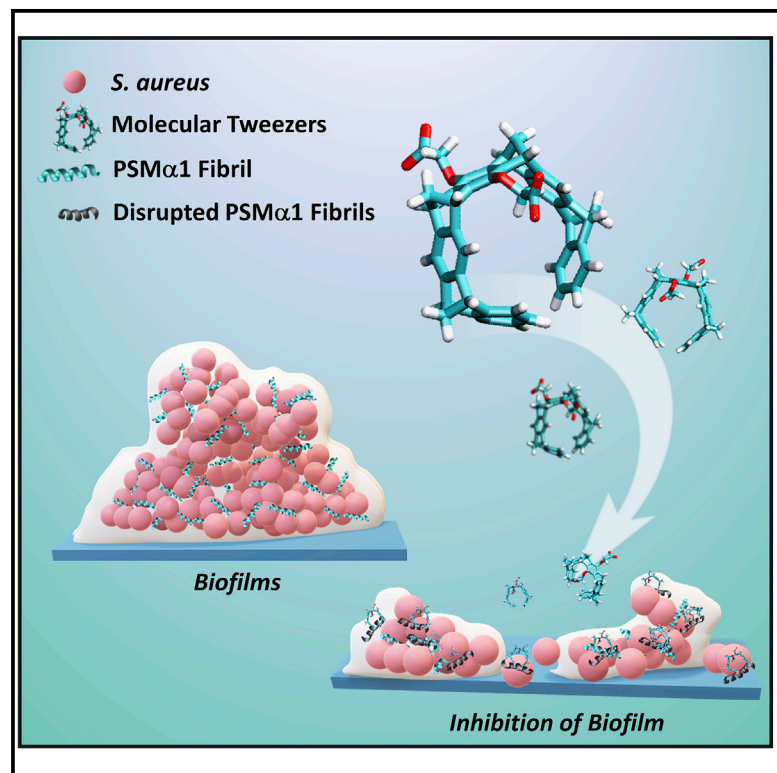


# Cell Chemical Biology

## Inhibition of *Staphylococcus aureus* biofilm-forming functional amyloid by molecular tweezers

### Graphical abstract



### Authors

Ravit Malishev, Nir Salinas, James Gibson, ..., Meytal Landau, Gal Bitan, Raz Jelinek

### Correspondence

razj@bgu.ac.il

### In brief

Malishev et al. present innovative “molecular tweezers” capable of inhibiting biofilm formation of *S. aureus*. Comprehensive structural, biophysical, and theoretical analyses reveal distinct effects of the tweezers upon assembly of the PSM $\alpha$ 1 functional amyloid, which is the main scaffolding peptide of the bacterial biofilm.

### Highlights

- Molecular tweezers inhibit *S. aureus* biofilms while not adversely affecting viability
- The tweezers inhibit fibrillation of PSM $\alpha$ 1, an amyloid peptide in the biofilm matrix
- Structural analysis shows distinct fibril inhibition mechanisms by the tweezers
- Tweezers disrupt biofilms and reduce virulence of antibiotic-resistant bacteria

Article

# Inhibition of *Staphylococcus aureus* biofilm-forming functional amyloid by molecular tweezers

Ravit Malishev,<sup>1</sup> Nir Salinas,<sup>3</sup> James Gibson,<sup>5</sup> Angela Bailey Eden,<sup>5</sup> Joel Mieres-Perez,<sup>6</sup> Yasser B. Ruiz-Blanco,<sup>6</sup> Orit Malka,<sup>1</sup> Sofiya Kolusheva,<sup>2</sup> Frank-Gerrit Klärner,<sup>7</sup> Thomas Schrader,<sup>7</sup> Elsa Sanchez-Garcia,<sup>6</sup> Chunyu Wang,<sup>5</sup> Meytal Landau,<sup>3,4</sup> Gal Bitan,<sup>8,9</sup> and Raz Jelinek<sup>1,2,\*</sup>

<sup>1</sup>Department of Chemistry, Ben Gurion University of the Negev, Beer Sheva 84105, Israel

<sup>2</sup>Ilse Katz Institute for Nanotechnology, Ben Gurion University of the Negev, Beer Sheva 84105, Israel

<sup>3</sup>Department of Biology, Technion-Israel Institute of Technology, Haifa 3200003, Israel

<sup>4</sup>European Molecular Biology Laboratory (EMBL), 22607 Hamburg, Germany

<sup>5</sup>Center for Biotechnology and Interdisciplinary Studies, Department of Biological Sciences, Rensselaer Polytechnic Institute, Troy, NY 12180, USA

<sup>6</sup>Department of Computational Biochemistry, University of Duisburg-Essen, Universitätsstrasse 2, 45141 Essen, Germany

<sup>7</sup>Faculty of Chemistry, University of Duisburg-Essen, Essen, Germany

<sup>8</sup>Department of Neurology, David Geffen School of Medicine, Brain Research Institute, and Molecular Biology Institute, University of California, Los Angeles, Los Angeles, CA, USA

<sup>9</sup>Lead contact

\*Correspondence: [razj@bgu.ac.il](mailto:razj@bgu.ac.il)

<https://doi.org/10.1016/j.chembiol.2021.03.013>

## SUMMARY

Biofilms are rigid and largely impenetrable three-dimensional matrices constituting virulence determinants of various pathogenic bacteria. Here, we demonstrate that molecular tweezers, unique supramolecular artificial receptors, modulate biofilm formation of *Staphylococcus aureus*. In particular, the tweezers affect the structural and assembly properties of phenol-soluble modulin  $\alpha 1$  (PSM $\alpha 1$ ), a biofilm-scaffolding functional amyloid peptide secreted by *S. aureus*. The data reveal that CLR01, a diphosphate tweezer, exhibits significant *S. aureus* biofilm inhibition and disrupts PSM $\alpha 1$  self-assembly and fibrillation, likely through inclusion of lysine side chains of the peptide. In comparison, different peptide binding occurs in the case of CLR05, a tweezer containing methylenecarboxylate units, which exhibits lower affinity for the lysine residues yet disrupts *S. aureus* biofilm more strongly than CLR01. Our study points to a possible role for molecular tweezers as potent biofilm inhibitors and antibacterial agents, particularly against untreatable biofilm-forming and PSM-producing bacteria, such as methicillin-resistant *S. aureus*.

## INTRODUCTION

Bacterial biofilms are integrated communities of cells consisting of one or more species joined in an extracellular polymeric matrix. Biofilms strengthen bacterial virulence by enabling bacterial cells to adhere efficiently to surfaces and shielding the cells from both host immune molecules and antibiotics (Bridier et al., 2011; Hall-Stoodley et al., 2004). The biofilm matrix contains polysaccharides, DNA, and proteins forming a highly impenetrable layer under which the bacterial cells thrive (Limoli et al., 2015; Satpathy et al., 2016). Several bacterial species secrete proteins that form amyloid-like fibrils, resembling amyloids involved in proteinopathies (Jucker and Walker, 2013), which serve as building blocks for biofilm scaffolding (Blanco et al., 2012; Taglialegna et al., 2016). Other functional amyloids mediate bacterial communication during biofilm assembly (Chiti and Dobson, 2006; Malishev et al., 2018; Romero et al., 2010; Tayeb-Fligelman et al., 2017). Thus, development of anti-amyloid substances that can inhibit biofilm formation and/or disrupt biofilm constituents is a

promising strategy for combating bacterial infections. In particular, antivirulence compounds that inhibit biofilm formation but not bacterial growth may induce less resistance compared with conventional antibiotics. This quest, however, is difficult because of the exceptional resilience of biofilm networks, often reducing the efficacy of antibiotic compounds (Flemming et al., 2016; Olsen, 2015).

*Staphylococcus aureus* is a well-known pathogenic, Gram-positive bacterium. Infections associated with *S. aureus* in the United States have an estimated mortality rate of above 25% (up to 40% in case of drug-resistant *S. aureus* strains [Bridier et al., 2011]). *S. aureus* infections also cause a high number of hospitalizations and significant medical costs (Mehlin et al., 1999; Rubin et al., 1999). The magnitude of the problem has been enhanced even more in 2020 due to the COVID-19 pandemic (Cusumano et al., 2020; Punjabi et al., 2020; Spoto et al., 2020). *S. aureus* generates extensive biofilm structures that contribute to its pathogenicity, conferring shielding and thereby antibiotic resistance. *S. aureus* secretes functional

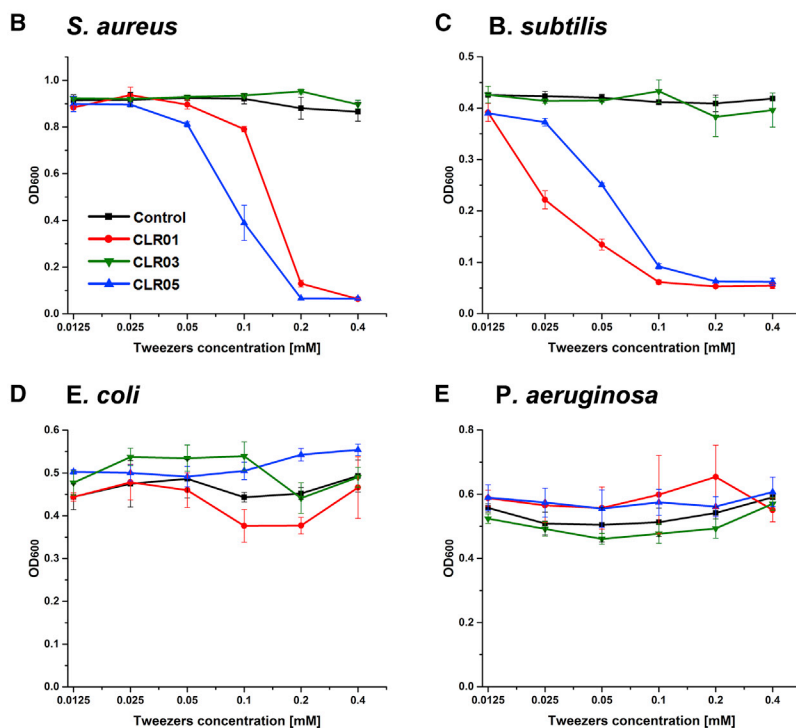
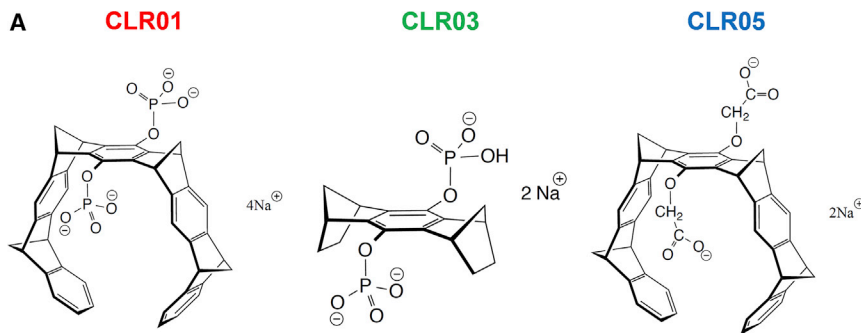


**Figure 1. Effects of the molecular tweezers on bacterial viability**

(A) Molecular structures of the tweezers. The compounds are partially protonated at physiologic pH.

(B–E) Dose-dependent effects of CLR01, CLR03, and CLR05 on the viability of (B) *S. aureus*, (C) *B. subtilis*, (D) *E. coli*, and (E) *P. aeruginosa*. Bacteria were grown for ~6 h in the absence or presence of increasing tweezer concentrations, and cell concentrations were determined by measuring absorbance at 600 nm. Data are presented as the mean  $\pm$  SD of three replicates.

abnormally self-assembling peptide and protein molecules. As such, CLR01 has been shown both to inhibit pathologic protein aggregation and to disintegrate mature fibrils (Lump et al., 2015; Prabhudesai et al., 2012; Sinha et al., 2011). CLR01 was found to inhibit the self-assembly and toxicity of multiple pathogenic proteins, including amyloid  $\beta$  protein, tau, and  $\alpha$ -synuclein (Bengoa-Vergniory et al., 2020; Despres et al., 2019; Di et al., 2021; Prabhudesai et al., 2012; Sinha et al., 2011). In particular, this tweezer intimately remodeled the assembly process, inducing formation of non-toxic and non-amyloidogenic structures that could be effectively degraded by natural cellular clearance mechanisms (Monaco et al., 2020; Prabhudesai et al., 2012; Xu et al., 2017).

Here, we investigate the impact of CLR01 and a less studied derivative called CLR05 (Figure 1A) on *S. aureus* biofilms and the biofilm-framework peptide PSM $\alpha$ 1. CLR01 and CLR05 share a similar structure but differ in the nature

of the negatively charged groups. As illustrated in Figure 1A, CLR01 has two phosphate groups whereas in CLR05, the negatively charged groups are O-methylene carboxylates. Previous studies have shown that the amyloid inhibitory activity of CLR05 is substantially weaker than that of CLR01, ascribed to partial occupation of the tweezer's cavity by the O-CH<sub>2</sub>-COO<sup>-</sup> groups, substantially reducing the ability of the compound to accommodate the side chains of lysine residues in target peptides (Schrader et al., 2016; Weil et al., 2020). A "truncated" phosphate-containing derivative, CLR03 (Figure 1A), which only forms electrostatic interactions through the two phosphate units, was included as a negative control.

amyloids called phenol-soluble modulins (PSMs) (Cheung et al., 2014), which trigger inflammatory responses, lyse human cells, and have been linked to the pronounced virulence of methicillin-resistant *S. aureus* (MRSA) (Otto, 2014; Queck et al., 2009). PSM $\alpha$ 1, a prominent member of the PSM peptide family, is particularly important for *S. aureus* biofilm assembly and structure, forming ultra-stable cross- $\beta$ -amyloid fibrils (Salinas et al., 2018; Schwartz et al., 2012). "Molecular tweezers" have been shown to significantly modulate the assembly properties of various amyloidogenic proteins (Attar and Bitan, 2014; Schrader et al., 2016). A lysine-binding tweezer denoted CLR01 (Figure 1A), for example, has been shown to be a powerful modulator of amyloid self-assembly and an inhibitor of the toxicity of multiple amyloidogenic proteins (Attar and Bitan, 2014; Schrader et al., 2016). The mechanism of action of CLR01 largely depends on its unique ability to draw the cationic side chains of exposed lysine residues into the interior of its cavity. This process is reversible and highly dynamic; it disrupts electrostatic and hydrophobic interactions among

The experimental data demonstrate that CLR01 and CLR05 inhibit both bacterial growth and biofilm formation of *S. aureus*. Importantly, we also discovered that these molecular tweezers interfere with the solution secondary structure and fibrillation of PSM $\alpha$ 1. Notably, CLR01 and CLR05 induced morphological changes and disintegration of mature PSM $\alpha$ 1 fibrils, suggesting that they can be used for treatment of existing infections. In

contrast, CLR03 did not affect *S. aureus* biofilms and had minor impact on PSM $\alpha$ 1 structure and assembly properties, as expected. The fluorescence titration and nuclear magnetic resonance (NMR) experiments reveal distinct inhibition mechanisms for CLR01 and CLR05, with the NMR analysis pointing to interactions of CLR01's side arms with the lysine residues of PSM $\alpha$ 1. Overall, our work points to the potential of molecular tweezers as agents against bacterial biofilms in general and those of *S. aureus* in particular.

## RESULTS AND DISCUSSION

To evaluate the impact of the molecular tweezers on bacterial viability and growth, we determined the growth curves of several Gram-positive and Gram-negative bacterial species in the absence or presence of CLR01, CLR03, or CLR05 (Figures 1B–1E). CLR01 (Figure 1, red lines) attenuated the growth of the Gram-positive bacterium *S. aureus* (at tweezer concentrations >50  $\mu$ M, and a half inhibitory concentration [IC<sub>50</sub>] of approximately 130  $\mu$ M, Figure 1B) and *Bacillus subtilis* (at concentrations >12.5  $\mu$ M, IC<sub>50</sub> of 25  $\mu$ M, Figure 1C) dose dependently, but not of the Gram-negative bacteria *Escherichia coli* (Figure 1D) or *Pseudomonas aeruginosa* (Figure 1E). CLR05 also inhibited growth of the two Gram-positive bacteria (Figures 1B and 1C, blue curves), while the inhibition capacity of CLR05 was reversed in comparison with CLR01. Specifically, CLR05 had stronger inhibitory effect than CLR01 for *S. aureus* (IC<sub>50</sub> of around 90  $\mu$ M) but lesser growth inhibition in the case of *B. subtilis* (IC<sub>50</sub> of 70  $\mu$ M, Figures 1B and 1C). The lack of antibacterial activity of the tweezers toward Gram-negative bacteria may be ascribed to electrostatic repulsion between the molecules and the ubiquitous negative lipopolysaccharide (LPS) moieties on the surface of these bacteria (Doerrler, 2006; Zhang et al., 2013). The absence of antibacterial activity of CLR03 toward both Gram-negative and Gram-positive bacteria (green lines in Figures 1B–1E) attests to the significance of the hydrophobic side arms of the tweezers for their antibacterial activities.

To characterize further the antibacterial selectivity of CLR01 and CLR05 toward Gram-positive bacteria, we examined the effect of the tweezers on *S. aureus* biofilm, as this largely impregnable matrix constitutes a fundamental virulence determinant of this bacterium (and other Gram-positive bacterial strains). Figure 2A depicts reconstructed confocal fluorescence microscopy images recorded after incubation of *S. aureus* with CLR01, CLR03, or CLR05, each at a concentration of 50  $\mu$ M, at 37°C for 24 h. Importantly, at this concentration the tweezers had little or no effect on the proliferation of *S. aureus* (Figure 1B). The images in Figure 2A, showing bacterial cells (green color) embedded within biofilm matrices (Yaniv et al., 2017), reveal pronounced disruption of *S. aureus* biofilm assembly by CLR01 and CLR05, whereas no discernible effect on biofilm integrity was observed for CLR03. Consistent with the more significant antibacterial effect of CLR05 against *S. aureus* (Figure 1B), Figure 2A shows a stronger biofilm inhibition by this tweezer. The dramatic inhibitory effects of CLR01 and CLR05 reflect disruption of the biofilm rather than an antibacterial effect because as shown in Figure 1B, the tweezers hardly affected *S. aureus* viability at the concentration employed in the biofilm-inhibition assay. Additional experiments demonstrated inhibition of *S. aureus* biofilm

formation by CLR01 and CLR05 also at 25  $\mu$ M, although at this concentration biofilm disruption was apparent at 12 h but biofilm growth resumed after 24 h (Figure S1).

To test whether biofilm inhibition by the tweezers occurred also in the physiological milieu and was potentially affected by the presence of other proteins and biological molecules, we further evaluated the inhibitory effects of the tweezers on *S. aureus* biofilm in 10% mouse serum using scanning electron microscopy (SEM; Figure 2B). The SEM image of the control sample shows a thick biofilm consisting of multilayered bacterial cells embedded within the biofilm matrix (Hall-Stoodley et al., 2004). Similar to the confocal microscopy images in Figure 2A, incubation of the bacterial cells with CLR01 and CLR05 resulted in significant reduction of biofilm mass and dispersion of bacterial cells, while CLR03 did not have a noticeable effect upon the biofilm (Figures 2B and S2A). Similar results were also recorded in the case of bacterial growth in mouse blood cells (Figure S2B). Together, the microscopy data in Figures 2B, S2A, and S2B demonstrate that tweezer-induced *S. aureus* biofilm inhibition was not disrupted by the presence of constituents such as blood proteins.

Complementing the fluorescence microscopy mapping, the effects of tweezer concentrations on *S. aureus* biofilm biomass stained with crystal violet were quantified (Figures 2C and 2D). The data confirmed the dose-dependent inhibitory effects of CLR01 and CLR05 and the lack of biofilm disruption by CLR03. Importantly, the quantitative analysis in Figure 2D demonstrates that biofilm disruption by both CLR01 and CLR05 already occurs at 25  $\mu$ M, i.e., at a concentration in which the tweezers do not affect bacterial viability (Figure 1B).

To elucidate the possible mechanism and molecular targets pertaining to the intriguing effects of the tweezers upon *S. aureus* growth and biofilm formation, we carried out comprehensive experimental and computational analyses (Figures 3, 4, 5, 6, and 7). We first determined whether the inhibitory mechanism involved modulation of membrane interactions of PSM $\alpha$ 1 (Figures S3A and S3B). Importantly, experiments utilizing bacterial membrane mimics through application of fluorescence anisotropy (Figure S3A) and Förster resonance energy transfer (Figure S3B) indicated no effect of the tweezers upon membrane interactions of the peptide. Figure 3 highlights the effects of the tweezers on PSM $\alpha$ 1  $\beta$ -sheet formation kinetics using the thioflavin T (ThT)-fluorescence assay (Figure 3A) and aggregate morphology by transmission electron microscopy (TEM; Figure 3B). PSM $\alpha$ 1 alone featured a typical ThT-fluorescence curve corresponding to fibril assembly, characterized by a lag time of  $\sim$ 6 h followed by a rapid increase of the fluorescence emission until a plateau was observed after 9 h. CLR01 induced the largest effect on both the ThT lag time prior to fluorescence increase and on signal intensity, almost completely inhibiting ThT fluorescence at both 1:1 and 1:5 PSM $\alpha$ 1/CLR01 molar ratios (Figure 3Ai). CLR05, in comparison, showed a dose-dependent effect on the ThT-fluorescence signal, reducing ThT intensity 2-fold at a 1:1 PSM $\alpha$ 1/CLR01 molar ratio, and affecting a nearly total inhibition at a 1:5 PSM $\alpha$ 1/CLR01 ratio (Figure 3Aii). Similar inhibitory effects were observed when the PSM $\alpha$ 1 solutions were seeded with preformed fibrils (data not shown).

Surprisingly, CLR03 gave rise to  $\sim$ 60% reduction of ThT fluorescence in both PSM $\alpha$ 1/CLR03 molar ratios (Figure 3Aiii).

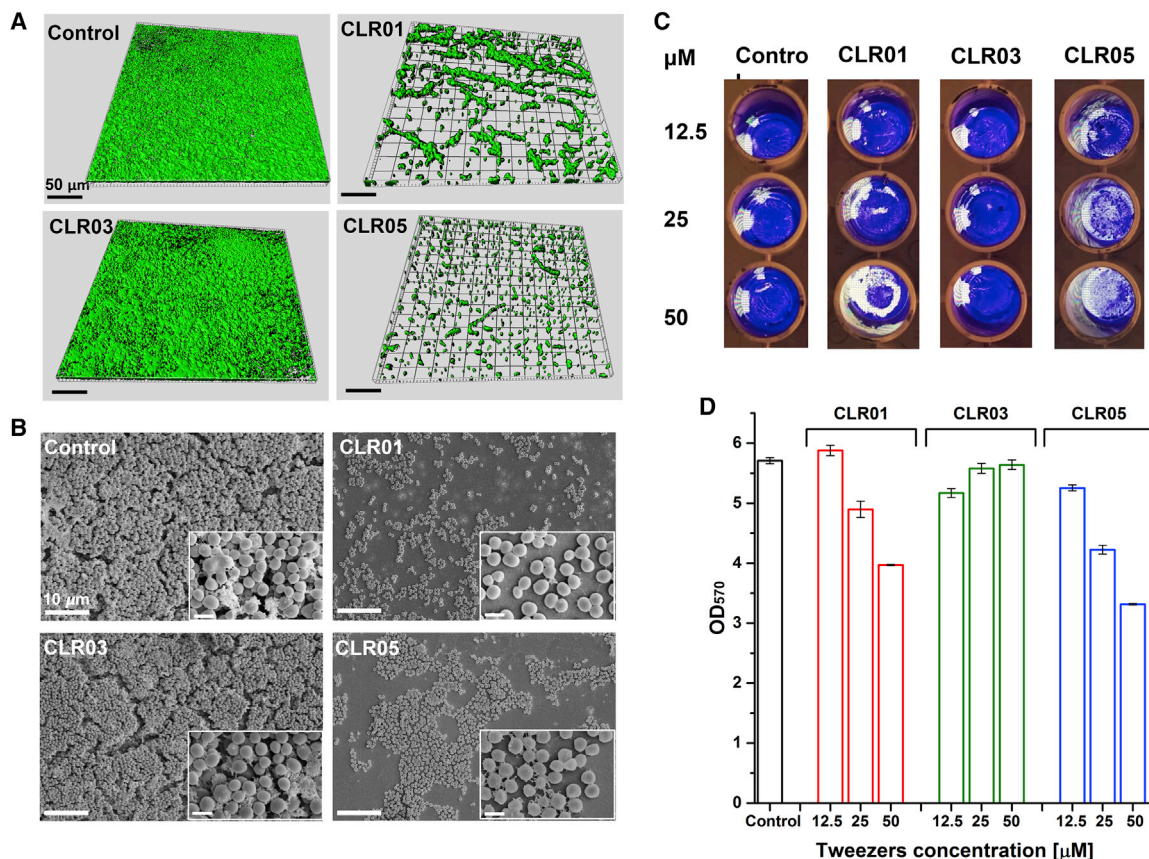


**Figure 2. Inhibition of *S. aureus* biofilms formation by the molecular tweezers**

(A) 50 μM CLR01, CLR03, or CLR05 were added to *S. aureus* cultures at  $t = 0$ .

Biofilm images showing viable cells stained in green using the LIVE/DEAD BacLight Bacterial Viability Kit. The images were recorded after 24-h incubation using confocal fluorescence microscopy (excitation/emission: 485 nm/498 nm). Scale bars, 50 μm.

(B) Scanning electron microscopy (SEM) micrographs of *S. aureus* biofilms grown in 10% mouse serum for 24 h. Scale bars in the magnified images represent 1 μm.

(C) Photographs of the wells in which *S. aureus* cells were cultured overnight in the absence or presence of tweezers and stained with crystal violet (blue) indicating biofilm formation. The white areas account for well areas not coated with biofilm.

(D) Optical density corresponding to biofilm stained with crystal violet. Tweezer concentrations were: 12.5, 25, and 50 μM. Data are presented as the mean ± SD of three replicates. \* $p < 0.05$  compared with control (black bar).

Interestingly, CLR03 shortened the lag time compared with PSM $\alpha$ 1 alone. This result stands in contrast to typical amyloid inhibitors, many of which increase the fibrillation lag time or completely abolish ThT signals (Borana et al., 2014). Experiments designed to test whether free lysines in the solution interfered with the inhibitory effects of the tweezers (through putative “scavenging” of the tweezer molecules) indicated that an excess of free lysines did not impede inhibition of fibril formation by the tweezers (Figure S4A). This result suggests that gentle, labile binding of the tweezers to the lysines in PSM $\alpha$ 1 is enough to prevent its aggregation; in particular, the competition by free Lys is not strong because the binding itself is not strong. Indeed, the exposure of lysine residues in varied self-assembled amyloidogenic proteins allows molecular tweezers to selectively remodel the misfolding and aggregation of such proteins, thereby eliminating toxic oligomers and aggregates, forming instead non-toxic and clearance-amenable aggregates (Malik et al., 2018).

The distinct inhibition effects of the tweezers on PSM $\alpha$ 1 fibrillation were further analyzed using TEM (Figures 3B and 3C). Echoing the ThT data (Figure 3A), TEM analysis revealed that CLR01 reduced the abundance of the fibrils substantially, giving rise to disparate, short fibrils. In contrast, CLR05/PSM $\alpha$ 1 at 1:1 molar ratio induced formation of “bundles” of short fibrils, distinct from the abundant, long fibrils formed by PSM $\alpha$ 1 alone. At 1:5 molar ratio (PSM $\alpha$ 1/CLR05), only a few fibrils were observed, in accordance with the large reduction in the ThT signal (Figure S4B). CLR03 induced a small, albeit distinguishable effect on PSM $\alpha$ 1, yielding shorter PSM $\alpha$ 1 upon incubation with the peptide at 1:1 molar ratio (Figure 3B) and gave rise to fibrils together with amorphous aggregates at 1:5 molar ratio (PSM $\alpha$ 1/CLR03, Figure S4B).

We also investigated whether CLR01, CLR03, or CLR05 could dissociate or otherwise alter the morphology of preassembled PSM $\alpha$ 1 fibrils. The molecular tweezers were added to mature PSM $\alpha$ 1 fibrils at a 1:1 molar ratio and the samples were

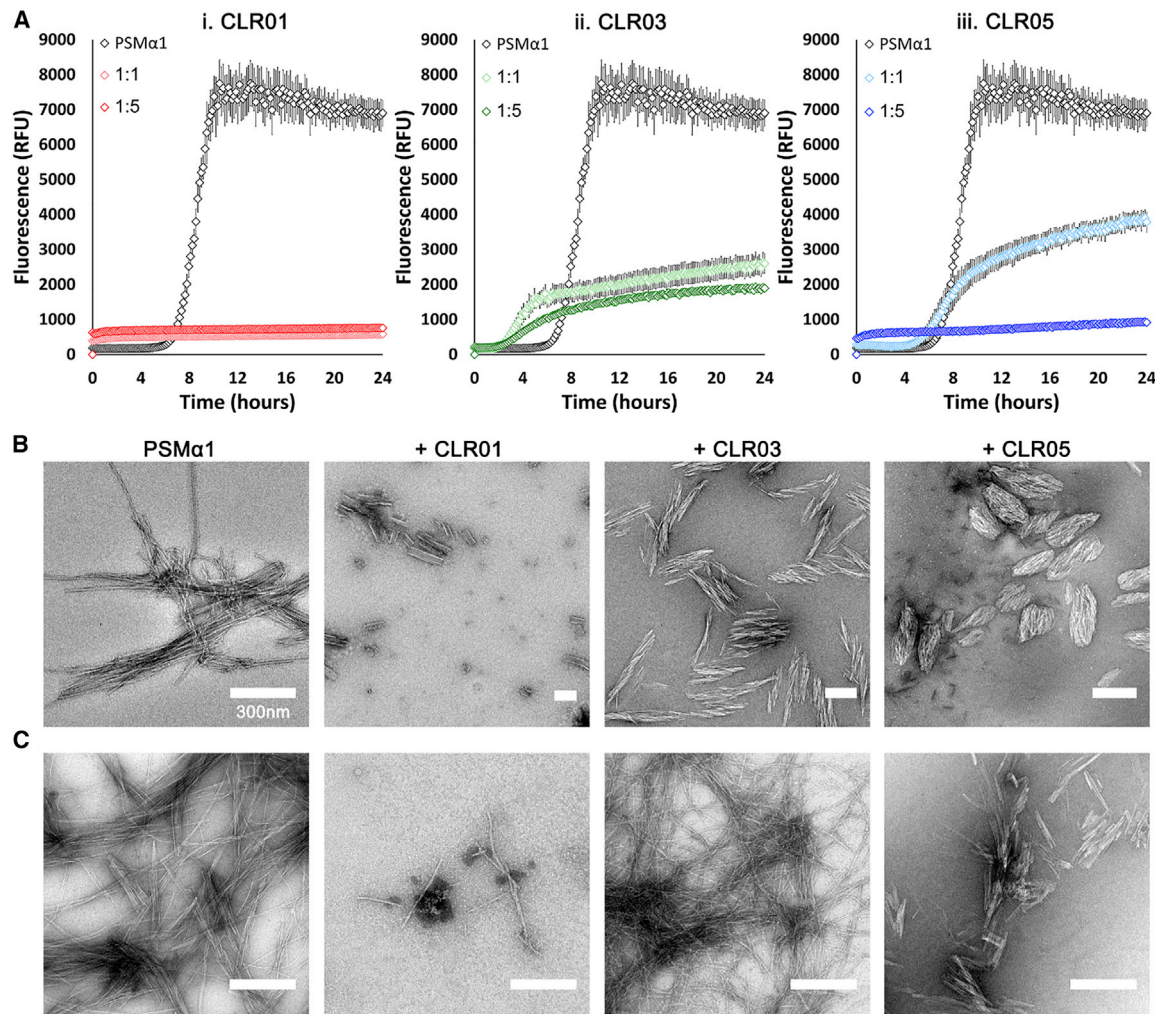


**Figure 3. Molecular tweezers inhibit PSM $\alpha$ 1 fibrillation and disaggregate preformed fibrils**

(A) PSM $\alpha$ 1  $\beta$ -sheet formation kinetics in the absence or presence of molecular tweezers at 1:1 and 1:5 molar ratio monitored by thioflavin T fluorescence. Data are presented as the mean  $\pm$  SD of three replicates.

(B) Transmission electron microscopy (TEM) micrographs of PSM $\alpha$ 1 at the end of the aggregation reactions in the absence or presence of equimolar molecular tweezer concentrations results in short scarce fibrils in the presence of CLR01 or multiple fibril bundles in the case of CLR03 and CLR05.

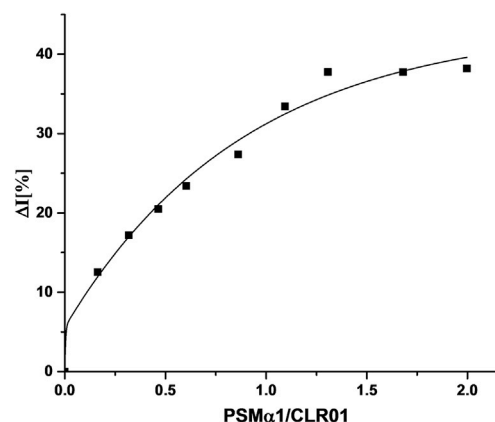
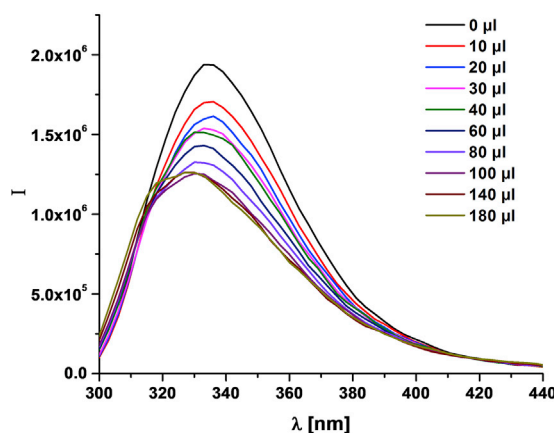
(C) TEM micrographs testing potential disaggregation of preformed PSM $\alpha$ 1 fibrils by CLR01, CLR03, or CLR05. The molecular tweezers were added at a 1:1 concentration ratio and further incubated for 24 h at 37°C. Scale bars, 300 nm.

visualized by TEM after 24 h of incubation (Figure 3C). The data demonstrate that CLR01, and to a lesser extent CLR05, disassembled PSM $\alpha$ 1 fibrils yielding less abundant, shorter fibrillar structures. CLR01, in particular, appeared to induce pronounced disassembly of PSM $\alpha$ 1, leaving only a few fibrils. CLR03 did not have a discernible effect. Previous studies have shown that CLR01 disassembled fibrils of A $\beta$ 40, A $\beta$ 42 (Sinha et al., 2011), and  $\alpha$ -synuclein (Prabhudesai et al., 2012), although those disassembly processes required excess CLR01 and occurred over weeks. In contrast, disaggregation of the human functional amyloid SEVI upon co-incubation with CLR01 occurred within a few hours (Lump et al., 2015). These data suggest that functional amyloids, such as PSM $\alpha$ 1 and SEVI, contain structural information that allows their facile disaggregation to serve the purpose of the organism using them, as opposed to abnormal amyloids,

such as those of A $\beta$  and  $\alpha$ -synuclein. Tweezer-induced PSM $\alpha$ 1 fibril disassembly was further illuminated by circular dichroism (Figure S4C), confirming the effects of CLR01 and CLR05.

Taken together, the ThT and TEM analyses underscore significant modulation of PSM $\alpha$ 1 fibrillation kinetics, reduction in fibril abundance, and altered fibril morphology by CLR01 and CLR05; and apparent fibril “bundling” specifically by CLR05. These results may account for the pronounced phenotypic impact of both CLR01 and CLR05 on *S. aureus* biofilms (Figure 2), as PSM $\alpha$ 1 is a major component of the biofilm scaffold of this bacteria species (Salinas et al., 2018). The much less pronounced structural disruption of PSM $\alpha$ 1 by CLR03 (ThT and TEM data in Figure 3) echo the weaker effect of this compound on *S. aureus* biofilm (Figure 2) and lack of antibacterial activity (Figures 1B–1E). This relationship is important because it testifies to the

**A CLR01**



**B CLR05**

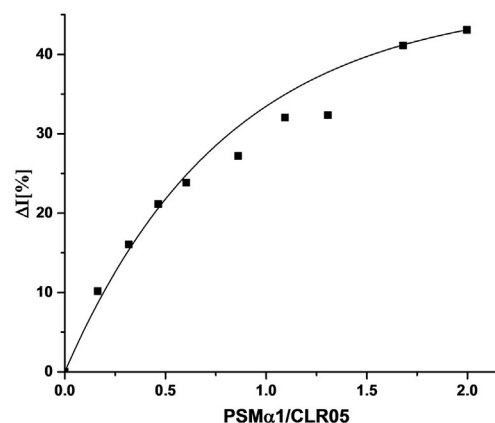
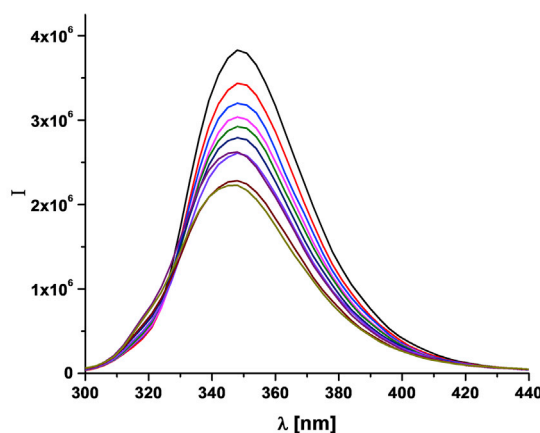


**Figure 4. Fluorometric titration of PSM $\alpha$ 1 into solutions of CLR01 or CLR05**

Fluorescence dependence of the emission band at  $\lambda_{em} = 336$  nm of CLR01 (A) and  $\lambda_{em} = 351$  nm of CLR05 (B) on the PSM $\alpha$ 1 concentration in 10 mM sodium phosphate (pH 7.4) ( $\lambda_{ex} = 285$  nm). The data were used to calculate the dissociation constant for each molecular tweezer.  $K_D$  values were calculated from the fluorometric titration experiments using a standard nonlinear regression by fitting host and guest concentrations.

significance of the tweezers' supramolecular organization in exerting biological activities. Additional experiments reveal that the tweezers also affect the fibrillation properties of PSM $\alpha$ 4 (Figure S5), another PSM constituent contributing to biofilm scaffoldings (Salinas et al., 2018), suggesting a broad-base effect of the tweezers.

To shed light on the bimolecular interactions between the molecular tweezers and PSM $\alpha$ 1, we applied fluorescence titration experiments utilizing the intrinsic fluorescence emission of the tweezers (Figure 4). Specifically, molecular tweezer derivatives with a central benzene bridge, such as CLR01 and CLR05, feature a strong emission band at  $\lambda_{em} \approx 330$  nm when excited at 285 nm, which is solvent and substituent dependent (Dutt et al., 2013). In the experiments presented in Figure 4, PSM $\alpha$ 1 was titrated into solutions of CLR01 or CLR05 while maintaining the molecular tweezers' concentration constant. Binding of either molecular tweezer to PSM $\alpha$ 1 led to partial quenching of the emission band. In the case of CLR01, the binding also caused a blue shift of the emission. No fluorescence emission was observed for CLR03. The dose-dependent fluorescence al-

lowed calculation of dissociation constants ( $K_D$ ) for the binding of each molecular tweezer to PSM $\alpha$ 1, as described previously (Dutt et al., 2013) (details pertaining to the titration experiments are outlined in Tables S1 and S2). The  $K_D$  value calculated for CLR01,  $11.1 \pm 0.7 \mu$ M, was similar to those found for this compound previously with lysine derivatives and short peptides (Talibersky et al., 2008). The blue shift of the emission peaks in the case of CLR01 (Figure 4A) likely accounts for direct interaction of the peptide with the aromatic rings of the tweezer. The dissociation constant calculated for CLR05 ( $K_D = 12.3 \pm 0.9 \mu$ M, Figure 4B) indicated similar affinity of CLR05 to the peptide. The absence of a blue shift upon titration of CLR05 with PSM $\alpha$ 1, however, points to a different binding mechanism consistent with the more pronounced inhibition of *S. aureus* biofilm (e.g., Figure 2).

To elucidate further the molecular details of the interactions between the tweezers and PSM $\alpha$ 1, we carried out two-dimensional heteronuclear NMR spectroscopy experiments. Figure 5 shows overlays of  $^1H$ - $^{13}C$  heteronuclear single quantum coherence (HSQC) spectra of PSM $\alpha$ 1 alone and its 1:1 mixture (molar

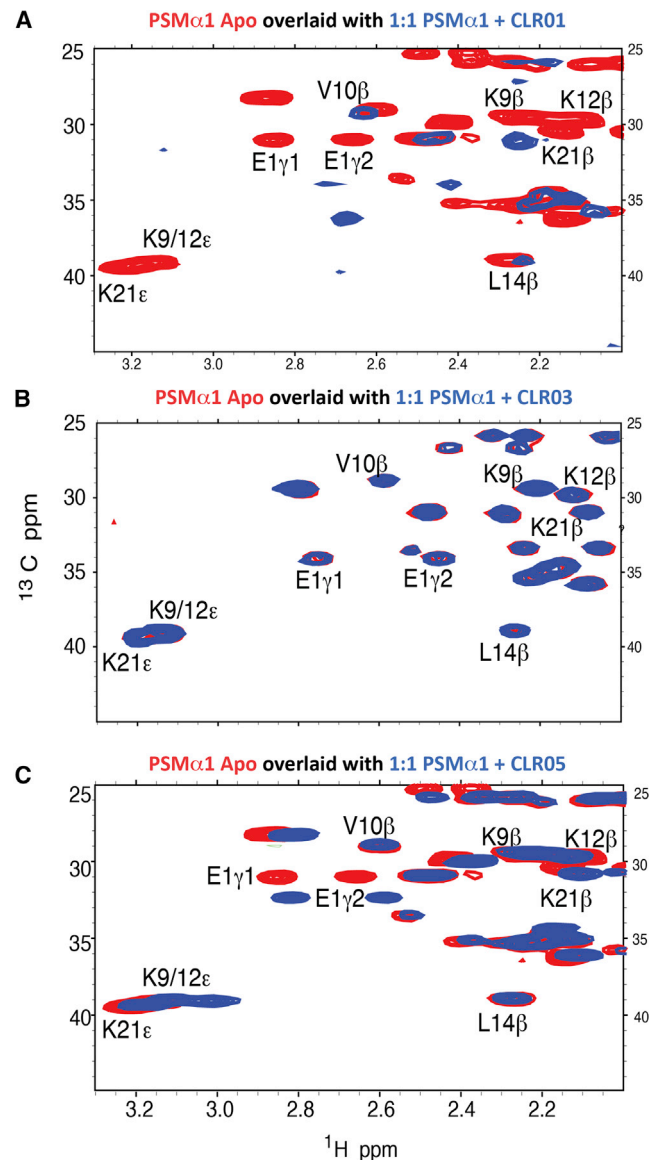


**Figure 5.** Overlay of  $^1\text{H}$ - $^{13}\text{C}$  HSQC spectra of apo PSM $\alpha$ 1 (red) and mixtures of PSM $\alpha$ 1 (blue) with each molecular tweezer at a 1:1 concentration ratio for selected residues

(A) CLR01; (B) CLR03; (C) CLR05. CLR01 shows strong interaction with the peptide, whereas CLR05 exhibits a much weaker binding and CLR03 shows no interaction.

ratios) with each tweezer. CLR01 had a major effect on PSM $\alpha$ 1 peak positions and peak intensities (Figure 5A, red versus blue peaks). Indeed, even at a ratio of 10:1 PSM $\alpha$ 1/CLR01, K9 already showed small yet significant chemical-shift change and a peak-intensity decrease (Figure S6). At a 1:1 ratio of PSM $\alpha$ 1/CLR01, the  $\epsilon$  and  $\beta$  peaks for all three lysine residues (K9, K12, and K21) were no longer visible (Figure 5A). The disappearance of these peaks is ascribed to dynamic line broadening when the lysine residues are efficiently complexed by CLR01. Importantly, CLR05 also produced changes in PSM $\alpha$ 1 peak intensities and chemical shifts (Figure 5C), supporting the notion that CLR05 binds to lysines and N-terminal amino group of residue E1 in

the peptide. Consistent with the minimal functional and structural effects of CLR03 (e.g., Figures 1, 2, and 3), this tweezer molecule had virtually no effect on the HSQC peaks of PSM $\alpha$ 1 (Figure 5B).

The strong perturbation of the NMR spectrum by CLR01 is consistent with the disruption of PSM $\alpha$ 1 aggregation (Figure 3) and pronounced inhibition of *S. aureus* biofilm formation by this tweezer derivative (Figure 2). The weaker but significant interactions between CLR05 and PSM $\alpha$ 1 lysines apparent in the NMR analysis (Figure 5C) possibly reflect interactions between the carboxylate moieties of CLR05 and the peptide occurring outside the tweezer's cavity (Dutt et al., 2013). This mode of binding is consistent with the absence of a blue shift in the fluorescence titration experiment (Figure 4B) and may underscore the distinctive inhibitory mechanism of this tweezer molecule.

Interestingly, the NMR resonances of E1, the N-terminal residue of PSM $\alpha$ 1, showed significant perturbation by both CLR01 and CLR05, indicating that the positively charged amino group at the N terminus may bind to the negative phosphate and carboxyl groups in CLR01 and CLR05, respectively. The lack of interaction between CLR03 and PSM $\alpha$ 1, apparent in the  $^1\text{H}$ - $^{13}\text{C}$  HSQC data in Figure 5B, echoes the lack of inhibition of *S. aureus* biofilm, although it does not fully explain the effects of CLR03 on ThT fluorescence (Figure 3A) and PSM $\alpha$ 1 morphology (Figure 3B). Weak inhibitory effects of CLR03 on the assembly of other proteins, presumably through electrostatic and/or  $\pi$ - $\pi$  interactions, have been reported previously (Herzog et al., 2015; Zheng et al., 2015), suggesting that in some cases the compound does not act purely as a negative control.

To further investigate the interactions of the tweezers with the PSM $\alpha$ 1 peptide and their effect on PSM $\alpha$ 1 self-assembly and fibrillation, we performed molecular dynamics simulations of PSM $\alpha$ 1-tweezers complexes (see computational details in STAR methods). We sampled complexes at a 1:1 ratio (PSM $\alpha$ 1/tweezers) in which the tweezers were placed either on K9 or K12 of the PSM $\alpha$ 1 peptide (Figure 6). Importantly, we found that the inclusion complexes of CLR01 with the PSM $\alpha$ 1 peptide were conserved during the simulations (Figures 6A and 6B), as evidenced by the average values of the geometrical parameters characterizing CLR01-Lys complexes (Table S3). A distinct scenario was observed for the PSM $\alpha$ 1-CLR05 system (Figures 6C–6F). In contrast to CLR01, CLR05 formed non-inclusion complexes with the PSM $\alpha$ 1 peptide. Specifically, while the inclusion complex of CLR05 accommodating K9 was conserved during the whole sampling, the inclusion complex between K12 and CLR05 was labile.

The simulations indicating that CLR05, unlike CLR01, establishes non-inclusion, i.e., more labile interactions with the lysine residues, evidence a weakened binding of CLR05 with respect to CLR01. This provides a rationale for the experimental data showing that CLR01 disrupts interactions between different units of the peptides to a larger extent than CLR05. The enhanced stability observed for the CLR01-PSM $\alpha$ 1 complexes is also in agreement with the strong effect of CLR01 reported in the NMR experiments. Specifically, the close proximity of the lysine side chain to the aromatic rings of CLR01 in the inclusion complex is in accordance with the blue shift observed in the fluorescence titration experiments.

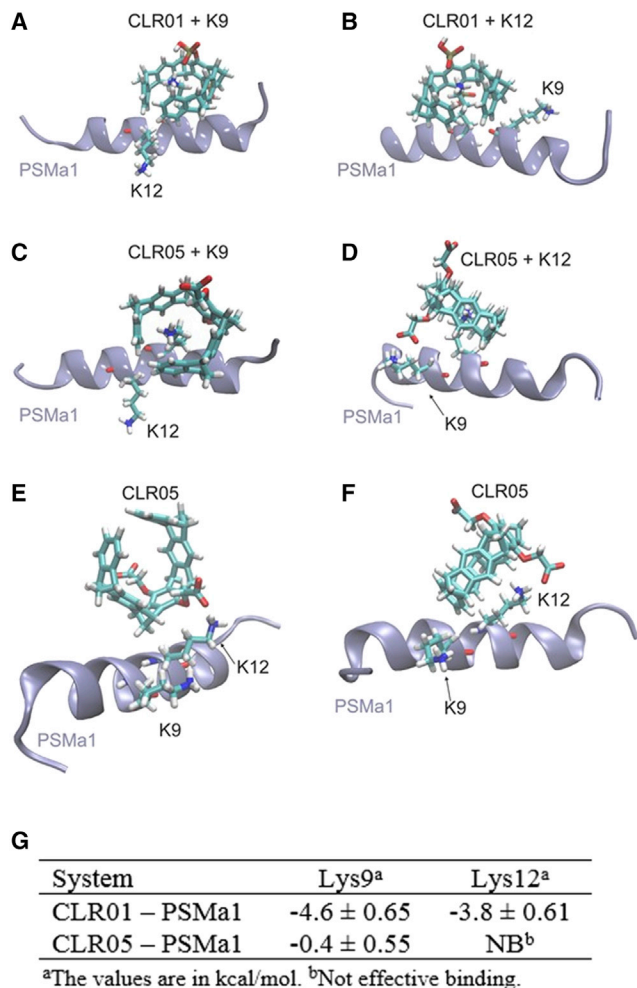


**Figure 6. CLR01 and CLR05 form inclusion complexes with the PSM $\alpha$ 1 peptide while CLR05 also forms non-inclusion structures**

(A) Inclusion complex of CLR01 with K9 (population of the main cluster of structures: 50.1%).  
 (B) Inclusion complex of CLR01 with K12 (population of the main cluster of structures: 51.7%).  
 (C) Inclusion complex of CLR05 with K9 (population of the main cluster of structures: 52.1%).  
 (D) Inclusion complex of CLR05 with K12 (population of the main cluster of structures: 32%).  
 (E and F) Non-inclusion interaction mode of CLR05 with K12 (populations of the main clusters of structures 22.4% and 5.3%, respectively).  
 (G) Binding free energies of inclusion complexes formed by CLR01 and CLR05 with PSM $\alpha$ 1 in a fibril-like conformation.

Several weak interactions are established between CLR05 and PSM $\alpha$ 1, not only between the carboxylate groups and the lysine residues but also involving the hydrophobic core of the tweezer and the hydrophobic groups of the peptide (Figures 6C–6F). However, the lysine residues complexed to CLR01 experience the effect of the five aromatic rings of the tweezer cavity simultaneously, while in the non-inclusion complexes with CLR05 the interaction with the aromatic rings is weakened since these rings are farther away from the lysine. Next, to provide insights into the inhibition of fibrillation by the tweezers, we calculated the binding free energies of both tweezers to a

PSM $\alpha$ 1 peptide in an extended conformation as model of a fibril-like configuration (see supplemental information: PSM $\alpha$ 1 peptide in fibril-like conformation and Figure S7). The results indicate that CLR01 is more effective in binding fibril-like structures of PSM $\alpha$ 1 than CLR05, thus potentially disrupting the PSM $\alpha$ 1 aggregates at early stages (Figure 6G and Tables S5–S7).

The lower predicted affinity of the inclusion complex of CLR05 supports a binding behavior of CLR05 which differs from that of CLR01 and cannot be fully explained by 1:1 complexes. Since the experiments show a stronger disruption of already formed fibrils by CLR01 in comparison with CLR05, we also studied the interactions of both tweezers using 8mer-clusters of PSM $\alpha$ 1 as fibril models (Figure 7). Each system (1:8 ratio with one PSM $\alpha$ 1 cluster and 8 molecules of tweezer), was placed in a box of explicit water as a solvent and investigated using Gaussian accelerated molecular dynamics simulations (see computational details in STAR methods). To study how many inclusion complexes were formed spontaneously between the fibril model and the tweezers, we placed the supramolecular ligands in the solvent close to the fibril model but not forming complexes (Figure 7A). During the simulations, a maximum of two tweezer molecules were observed to form, simultaneously, inclusion complexes with the cluster of peptides. Thus, the simulations show that the tweezers form inclusion complexes with the cluster of peptides in proportions 1:1 and 2:1 (Figures 7B and 7C; Table S4). The remaining tweezer molecules either stay in solution (Figure 7C, gray) or form non-inclusion complexes.

The inclusion complexes involve lysine residues at different chains of the model fibril (Figure 7). In the case of CLR05, Figure 7B shows that only a single tweezer molecule formed an inclusion complex with the cluster during the entire sampling (Table S4). The larger number of inclusion complexes formed by CLR01 (Figure 7C) is consistent with the stronger effect of this tweezer in the disruption of already formed fibrils. Interestingly, not all CLR01 molecules interacting with the cluster form inclusion complexes, and the “outer/non-inclusion” mode characteristic of CLR05 in the simulations with the peptide is also observed for CLR01 and the model fibril (Figure 7). This observation is presumably related to steric clashes in the crowded environment of the aggregate surface.

Based on the modeling analysis, we believe that the longer methyl carboxylate arms of CLR05 may dock onto PSM $\alpha$ 1 fibrils as opposed to CLR01, which caps lysines by cavity inclusion thereby leading to fibril disaggregation. In the calculated tweezer/peptide complexes the cavity of bound CLR05 is still open to accommodate additional guests in the vicinity of the bound lysine. This may direct the CLR05 molecule to adhere to the accessible side chains of non-polar amino acid residues such as isoleucine, valine, or even methionine for an additional hydrophobic effect and dispersive interactions.

## Conclusions

Our study explores the effects of molecular tweezers on *S. aureus* biofilm assembly and the functional amyloid PSM $\alpha$ 1, which comprises the primary scaffold of the biofilm matrix. The experiments demonstrate that CLR01 and CLR05 potently inhibit *S. aureus* biofilm formation and fibrillation of PSM $\alpha$ 1, whereas CLR03 (lacking the extended side walls of CLR01 and CLR05)

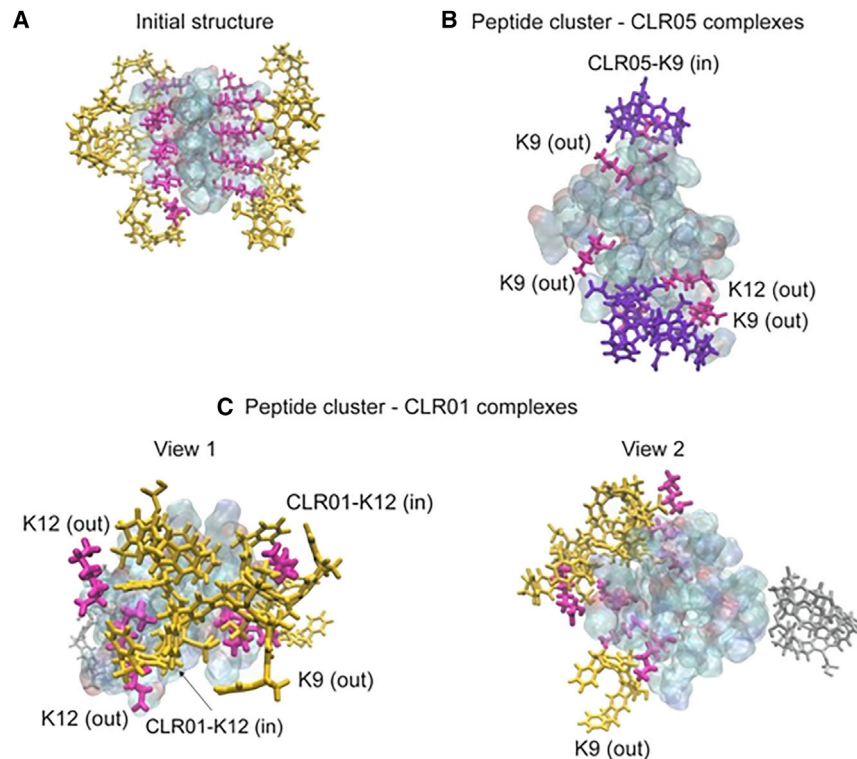


**Figure 7. Complexes between the tweezers and the PSM $\alpha$ 1 fibril model**

(A) The initial configuration of the system, in which the tweezers do not encapsulate any lysine residue of the fibril model (peptide cluster), is shown with CLR01 as representative case. (B) CLR05-fibril model interactions. CLR05 molecules are indicated in violet. In all panels, the fibril model is shown as transparent surface and the lysine residues interacting with the tweezers are highlighted in pink. The type of complex formed is described as “in” for inclusion complexes and “out” for non-inclusion complexes. Ions and water molecules are omitted for clarity. (C) CLR01-fibril model interactions. Two views of the same structure are shown, in which CLR01 is depicted in yellow when interacting with the studied lysine residues of the fibril and in gray when it remains in the solvent, close to the fibril but not interacting with the target residues.

does not affect biofilm formation and has a relatively minor impact on PSM $\alpha$ 1 assembly. These data demonstrate that although CLR01 and CLR05 appear to utilize different mechanisms, their hydrophobic side arms are important for their inhibitory activity.

The inhibitory activity of CLR01 is mediated primarily through inclusion of Lys side chains of PSM $\alpha$ 1 inside its cavity, as demonstrated by the NMR analysis, whereas CLR05 likely binds PSM $\alpha$ 1 outside of the tweezer’s cavity, possibly accounting for the more potent inhibition of *S. aureus* biofilm formation and reduced viability compared with CLR01. Both tweezers show potent, dose-dependent antibacterial activity and, importantly, at a lower concentration-antibiofilm activity. Thus, molecular tweezers may constitute a platform for disrupting the assembly of bacterial functional amyloid peptides and bacterial biofilms, supplementing antibiotic treatment of bacterial infection. This is especially important in light of the urgent need to find novel and effective ways for combating treatment-resistant bacterial infections, such as those induced by MRSA, which are increasingly prevalent in hospitals globally and currently untreated. Importantly, bacterial growth and biofilm inhibition by CLR05 may involve additional biological mechanisms other than structural effects upon PSM $\alpha$ 1. For example, possible interference of the molecular tweezers in quorum sensing cascades, which are complex genetic pathways affecting cell-cell communication and biofilm proliferation, may occur.

## SIGNIFICANCE

**This study reveals that diphosphate “molecular tweezers” block biofilm formation, the core virulence factor of *Staph-***

***lococcus aureus*, a prominent pathogenic bacterium often displaying multidrug resistance. Comprehensive functional, structural, and computational analyses trace the tweezer-mediated biofilm-inhibition mechanism to disruption of assembly and fibrillation of phenol-soluble modulin  $\alpha$ 1 (PSM $\alpha$ 1), a biofilm-scaffolding amyloid peptide secreted by *S. aureus*. Our study points to a possible role for molecular tweezers as potent biofilm inhibitors and antibacterial agents, particularly promising for untreatable biofilm-forming and PSM-producing bacteria such as methicillin-resistant *S. aureus*.**

## STAR★METHODS

Detailed methods are provided in the online version of this paper and include the following:

- [KEY RESOURCES TABLE](#)
- [RESOURCE AVAILABILITY](#)
  - Lead contact
  - Materials availability
  - Data and code availability
- [EXPERIMENTAL MODEL](#)
  - *Ex vivo* animal studies
  - Bacterial strains and culture media
- [METHOD DETAILS](#)
  - Peptide preparations
  - Lipid vesicle preparation
  - Bacterial growth
  - Blood collection
  - Biofilm modulation activity

- Scanning electron microscopy (SEM)
- Quantitate biofilm analysis by crystal violet assay
- Thioflavin-T fluorescence fibrillation-kinetics assay
- Transmission electron microscopy
- Disintegration of mature fibrils
- Fluorescence titration
- NMR spectroscopy and titration
- Computational details
- Fluorescence anisotropy
- Förster resonance energy transfer (FRET)
- CD spectroscopy

● **QUANTIFICATION AND STATISTICAL ANALYSIS**

**SUPPLEMENTAL INFORMATION**

Supplemental information can be found online at <https://doi.org/10.1016/j.chembiol.2021.03.013>.

**ACKNOWLEDGMENTS**

The authors are grateful to Nitzan Shauloff (Ben Gurion University) for help with SEM imaging and graphical abstract design. We acknowledge Prof. Elena Voronov (Ben Gurion University) for her assistance with the mouse blood and mouse serum samples in the project. E.S.-G. was supported by the collaborative research center CRC 1093 “Supramolecular Chemistry on Proteins” and by Germany’s Excellence Strategy – EXC 2033–390677874 – RESOLV, both funded by the German Research Foundation (DFG). E.S.-G. also acknowledges the support of the Boehringer Ingelheim Foundation (Plus-3 Program) and computing time at the supercomputer Magnitude. G.B. acknowledges support by NIH/NIA grants R01AG050721 and RF1AG054000.

**AUTHOR CONTRIBUTIONS**

The manuscript was written through contributions of all authors. All authors have given approval to the final version of the manuscript.

**DECLARATION OF INTERESTS**

A patent related to the molecular tweezers has been awarded: G. Bitan, A. Shanmugam, A. Lomakin, T. Schrader, F.G. Klärner, P. Talbierski, J. Polkowska, F. Bastowski, S. Sinha, and S. Frautschy (2009) Molecular Tweezers for the Treatment of Amyloid-Related Diseases. International Patent No. PCT/US2010/026419, USA Patent No. 8,791,092, European Patent No. EP2403859 A2.

Received: October 16, 2020

Revised: January 19, 2021

Accepted: March 19, 2021

Published: April 13, 2021

**REFERENCES**

Attar, A., and Bitan, G. (2014). Disrupting self-assembly and toxicity of amyloidogenic protein oligomers by “molecular tweezers” —from the test tube to animal models. *Curr. Pharm. Des.* **20**, 2469–2483.

Bengoa-Vergniory, N., Faggiani, E., Ramos-Gonzalez, P., Kirkiz, E., Connor-Robson, N., Brown, L.V., Siddique, I., Li, Z., Vingill, S., Cioroch, M., et al. (2020). CLR01 protects dopaminergic neurons in vitro and in mouse models of Parkinson’s disease. *Nat. Commun.* **11**, 4885.

Bier, D., Rose, R., Bravo-Rodriguez, K., Bartel, M., Ramirez-Angueta, J.M., Dutt, S., Wilch, C., Klärner, F.-G., Sanchez-Garcia, E., and Schrader, T. (2013). Molecular tweezers modulate 14-3-3 protein-protein interactions. *Nat. Chem.* **5**, 234–239.

Blanco, L.P., Evans, M.L., Smith, D.R., Badtke, M.P., and Chapman, M.R. (2012). Diversity, biogenesis and function of microbial amyloids. *Trends Microbiol.* **20**, 66–73.

Borana, M.S., Mishra, P., Pissurlenkar, R.R., Hosur, R.V., and Ahmad, B. (2014). Curcumin and kaempferol prevent lysozyme fibril formation by modulating aggregation kinetic parameters. *Biochim. Biophys. Acta* **1844**, 670–680.

Bridier, A., Briandet, R., Thomas, V., and Dubois-Brissonnet, F. (2011). Resistance of bacterial biofilms to disinfectants: a review. *Biofouling* **27**, 1017–1032.

Cheung, G.Y., Joo, H.-S., Chatterjee, S.S., and Otto, M. (2014). Phenol-soluble modulins—critical determinants of staphylococcal virulence. *FEMS Microbiol. Rev.* **38**, 698–719.

Chiti, F., and Dobson, C.M. (2006). Protein misfolding, functional amyloid, and human disease. *Annu. Rev. Biochem.* **75**, 333–366.

Cusumano, J.A., Dupper, A.C., Malik, Y., Gavioli, E.M., Banga, J., Berbel Caban, A., Nadkarni, D., Obla, A., Vasa, C.V., Mazo, D., et al. (2020). *Staphylococcus aureus* bacteremia in patients infected with COVID-19: a case series. *Open Forum Infect. Dis.* **7**, ofaa518.

Darden, T., York, D., and Pedersen, L. (1993). Particle mesh Ewald: an  $N \cdot \log(N)$  method for Ewald sums in large systems. *J. Chem. Phys.* **98**, 10089–10092.

Despres, C., Di, J., Cantrelle, F.X., Li, Z., Huvent, I., Chambraud, B., Zhao, J., Chen, J., Chen, S., Lippens, G., et al. (2019). Major differences between the self-assembly and seeding behavior of heparin-induced- and in-vitro-phosphorylated tau and their modulation by potential inhibitors. *ACS Chem. Biol.* **14**, 1363–1379.

Di, J., Siddique, I., Li, Z., Malki, G., Hornung, S., Dutta, S., Hurst, I., Ishaaya, E., Wang, A., Tu, S., et al. (2021). The molecular tweezer CLR01 improves behavioral deficits and reduces tau pathology in P301S-tau transgenic mice. *Alzheimers Res. Ther.* **13**, 6.

Doerrler, W.T. (2006). Lipid trafficking to the outer membrane of Gram-negative bacteria. *Mol. Microbiol.* **60**, 542–552.

Dutt, S., Wilch, C., Gersthagen, T., Talbierski, P., Bravo-Rodriguez, K., Hanni, M., Sanchez-Garcia, E., Ochsenfeld, C., Klärner, F.-G., and Schrader, T. (2013). Molecular tweezers with varying anions: a comparative study. *J. Org. Chem.* **78**, 6721–6734.

Flemming, H.-C., Wengender, J., Szewzyk, U., Steinberg, P., Rice, S.A., and Kjelleberg, S. (2016). Biofilms: an emergent form of bacterial life. *Nat. Rev. Microbiol.* **14**, 563.

Fokkens, M., Schrader, T., and Klärner, F.-G. (2005). A molecular tweezer for lysine and arginine. *J. Am. Chem. Soc.* **127**, 14415–14421.

Hall-Stoodley, L., Costerton, J.W., and Stoodley, P. (2004). Bacterial biofilms: from the natural environment to infectious diseases. *Nat. Rev. Microbiol.* **2**, 95–108.

Herzog, G., Shmueli, M.D., Levy, L., Engel, L., Gazit, E., Klärner, F.G., Schrader, T., Bitan, G., and Segal, D. (2015). The lys-specific molecular tweezer, CLR01, modulates aggregation of the mutant p53 DNA binding domain and inhibits its toxicity. *Biochemistry* **54**, 3729–3738.

Humphrey, W., Dalke, A., and Schulten, K. (1996). VMD: visual molecular dynamics. *J. Mol. Graphics* **14**, 33–38.

Jorgensen, W.L., Chandrasekhar, J., Madura, J.D., Impey, R.W., and Klein, M.L. (1983). Comparison of simple potential functions for simulating liquid water. *J. Chem. Phys.* **79**, 926–935.

Jucker, M., and Walker, L.C. (2013). Self-propagation of pathogenic protein aggregates in neurodegenerative diseases. *Nature* **507**, 45–51.

Klauda, J.B., Venable, R.M., Freites, J.A., O’Connor, J.W., Tobias, D.J., Mondragon-Ramirez, C., Vorobyov, I., MacKerell, A.D., Jr., and Pastor, R.W. (2010). Update of the CHARMM all-atom additive force field for lipids: validation on six lipid types. *J. Phys. Chem. B* **114**, 7830–7843.

Limoli, D.H., Jones, C.J., and Wozniak, D.J. (2015). Bacterial extracellular polysaccharides in biofilm formation and function. *Microb. Biofilms*, 223–247.

Lump, E., Castellano, L.M., Meier, C., Seeliger, J., Erwin, N., Sperlich, B., Stürzel, C.M., Usmani, S., Hammond, R.M., and von Einem, J. (2015). A molecular tweezer antagonizes seminal amyloids and HIV infection. *eLife* **4**, e05397.

Malik, R., Di, J., Nair, G., Attar, A., Taylor, K., Teng, E., Klärner, F.-G., Schrader, T., and Bitan, G. (2018). Using molecular tweezers to remodel abnormal protein self-assembly and inhibit the toxicity of amyloidogenic proteins. In

Peptide Self-Assembly: Methods and Protocols, B.L. Nilsson and T.M. Doran, eds. (Springer), pp. 369–386.

Malishev, R., Abbasi, R., Jelinek, R., and Chai, L. (2018). Bacterial model membranes reshape fibrillation of a functional amyloid protein. *Biochemistry* 57, 5230–5238.

Mehlin, C., Headley, C.M., and Klebanoff, S.J. (1999). An inflammatory poly-peptide complex from *Staphylococcus epidermidis*: isolation and characterization. *J. Exp. Med.* 189, 907–918.

Monaco, A., Maffia, V., Sorrentino, N.C., Sambri, I., Ezhova, Y., Giuliano, T., Cacace, V., Nusco, E., De Risi, M., De Leonibus, E., et al. (2020). The amyloid inhibitor CLR01 relieves autophagy and ameliorates neuropathology in a severe lysosomal storage disease. *Mol. Ther.* 28, 1167–1176.

Olsen, I. (2015). Biofilm-specific antibiotic tolerance and resistance. *Eur. J. Clin. Microbiol. Infect. Dis.* 34, 877–886.

Otto, M. (2014). Phenol-soluble modulins. *Int. J. Med. Microbiol.* 304, 164–169.

Pang, Y.T., Miao, Y., Wang, Y., and McCammon, J.A. (2017). Gaussian accelerated molecular dynamics in NAMD. *J. Chem. Theor. Comput.* 13, 9–19.

Phillips, J.C., Braun, R., Wang, W., Gumbart, J., Tajkhorshid, E., Villa, E., Chipot, C., Skeel, R., Kalé, L., and Schulten, L. (2005). Scalable molecular dynamics with NAMD. *J. Comput. Chem.* 26, 1781–1802.

Phillips, J.C., Hardy, D.J., Maia, J.D., Stone, J.E., Ribeiro, J.V., Bernardi, R.C., Buch, R., Fiorin, G., Hémin, J., and Jiang, W. (2020). Scalable molecular dynamics on CPU and GPU architectures with NAMD. *J. Chem. Phys.* 153, 044130.

Prabhudesai, S., Sinha, S., Attar, A., Kotagiri, A., Fitzmaurice, A.G., Lakshmanan, R., Ivanova, M.I., Loo, J.A., Klärner, F.G., Schrader, T., et al. (2012). A novel "molecular tweezer" inhibitor of  $\alpha$ -synuclein neurotoxicity in vitro and in vivo. *Neurotherapeutics* 9, 464–476.

Punjabi, C.D., Madaline, T., Gendlina, I., Chen, V., Nori, P., and Pirofski, L.A. (2020). Prevalence of methicillin-resistant *Staphylococcus aureus* (MRSA) in respiratory cultures and diagnostic performance of the MRSA nasal polymerase chain reaction (PCR) in patients hospitalized with coronavirus disease 2019 (COVID-19) pneumonia. *Infect. Control. Hosp. Epidemiol.* 1–2.

Queck, S.Y., Khan, B.A., Wang, R., Bach, T.-H.L., Kretschmer, D., Chen, L., Kreiswirth, B.N., Peschel, A., DeLeo, F.R., and Otto, M. (2009). Mobile genetic element-encoded cytolysin connects virulence to methicillin resistance in MRSA. *PLoS Pathog.* 5, e1000533.

Romero, D., Aguilar, C., Losick, R., and Kolter, R. (2010). Amyloid fibers provide structural integrity to *Bacillus subtilis* biofilms. *Proc. Natl. Acad. Sci. U S A* 107, 2230–2234.

Roy, A., Kucukural, A., and Zhang, Y. (2010). I-TASSER: a unified platform for automated protein structure and function prediction. *Nat. Protoc.* 5, 725–738.

Rubin, R.J., Harrington, C.A., Poon, A., Dietrich, K., Greene, J.A., and Moiduddin, A. (1999). The economic impact of *Staphylococcus aureus* infection in New York City hospitals. *Emerg. Infect. Dis.* 5, 9.

Ruiz-Blanco, Y.B., and Sanchez-Garcia, E. (2020). CL-FEP: an end-state free energy perturbation approach. *J. Chem. Theor. Comput.* 16, 1396–1410.

Salinas, N., Colletier, J.-P., Moshe, A., and Landau, M. (2018). Extreme amyloid polymorphism in *Staphylococcus aureus* virulent PSM $\alpha$  peptides. *Nat. Commun.* 9, 3512.

Satpathy, S., Sen, S.K., Pattanaik, S., and Raut, S. (2016). Review on bacterial biofilm: an universal cause of contamination. *Biocatal. Agric. Biotechnol.* 7, 56–66.

Schrader, T., Bitan, G., and Klärner, F.G. (2016). Molecular tweezers for lysine and arginine—powerful inhibitors of pathologic protein aggregation. *Chem. Commun. (Camb)* 52, 11318–11334.

Schwartz, K., Syed, A.K., Stephenson, R.E., Rickard, A.H., and Boles, B.R. (2012). Functional amyloids composed of phenol soluble modulins stabilize *Staphylococcus aureus* biofilms. *PLoS Pathog.* 8, e1002744.

Sinha, S., Lopes, D.H., Du, Z., Pang, E.S., Shanmugam, A., Lomakin, A., Talbiersky, P., Tennstaedt, A., McDaniel, K., Bakshi, R., et al. (2011). Lysine-specific molecular tweezers are broad-spectrum inhibitors of assembly and toxicity of amyloid proteins. *J. Am. Chem. Soc.* 133, 16958–16969.

Spoto, S., Valeriani, E., Riva, E., De Cesaris, M., Tonini, G., Vincenzi, B., Locorriere, L., Beretta Anguissola, G., Lauria Pantano, A., Brando, E., et al. (2020). A *Staphylococcus aureus* coinfection on a COVID-19 pneumonia in a breast cancer patient. *Int. J. Gen. Med.* 13, 729–733.

Taglialegna, A., Lasa, I., and Valle, J. (2016). Amyloid structures as biofilm matrix scaffolds. *J. Bacteriol.* 198, 2579–2588.

Talbiersky, P., Bastkowski, F., Klärner, F.-G., and Schrader, T. (2008). Molecular clip and tweezer introduce new mechanisms of enzyme inhibition. *J. Am. Chem. Soc.* 130, 9824–9828.

Tayeb-Fligelman, E., Tabachnikov, O., Moshe, A., Goldshmidt-Tran, O., Sawaya, M.R., Coquelle, N., Colletier, J.-P., and Landau, M. (2017). The cytotoxic *Staphylococcus aureus* PSM $\alpha$ 3 reveals a cross- $\alpha$  amyloid-like fibril. *Science* 355, 831–833.

Towle, K.M., Lohans, C.T., Miskolzie, M., Acedo, J.Z., van Belkum, M.J., and Vederas, J.C. (2016). Solution structures of phenol-soluble modulins  $\alpha$ 1,  $\alpha$ 3, and  $\beta$ 2, virulence factors from *Staphylococcus aureus*. *Biochemistry* 55, 4798–4806.

Trusch, F., Kowski, K., Bravo-Rodríguez, K., Beuck, C., Sowislok, A., Wettig, B., Matena, A., Sanchez-Garcia, E., Meyer, H., and Schrader, T. (2016). Molecular tweezers target a protein-protein interface and thereby modulate complex formation. *Chem. Commun.* 52, 14141–14144.

Vanommeslaeghe, K., and MacKerell, A., Jr. (2015). CHARMM additive and polarizable force fields for biophysics and computer-aided drug design. *Biochim. Biophys. Acta* 1850, 861–871.

Weil, T., Groß, R.d., Röcker, A., Bravo-Rodríguez, K., Heid, C., Sowislok, A., Le, M.-H., Erwin, N., Dwivedi, M., and Bart, S.M. (2020). Supramolecular mechanism of viral envelope disruption by molecular tweezers. *J. Am. Chem. Soc.* 142, 17024–17038.

Xu, N., Bitan, G., Schrader, T., Klärner, F.G., Osinska, H., and Robbins, J. (2017). Inhibition of mutant  $\alpha$ B crystallin-induced protein aggregation by a molecular tweezer. *J. Am. Heart Assoc.* 6, e006182.

Yang, J., and Zhang, Y. (2015). I-TASSER server: new development for protein structure and function predictions. *Nucleic Acids Res.* 43, W174–W181.

Yaniv, K., Golberg, K., Kramarsky-Winter, E., Marks, R., Pushkarev, A., Bèjà, O., and Kushmaro, A. (2017). Functional marine metagenomic screening for anti-quorum sensing and anti-biofilm activity. *Biofouling* 33, 1–13.

Zhang, G., Meredith, T.C., and Kahne, D. (2013). On the essentiality of lipopolysaccharide to Gram-negative bacteria. *Curr. Opin. Microbiol.* 16, 779–785.

Zheng, X., Liu, D., Klärner, F.G., Schrader, T., Bitan, G., and Bowers, M.T. (2015). Amyloid  $\beta$ -protein assembly: the effect of molecular tweezers CLR01 and CLR03. *J. Phys. Chem. B* 119, 4831–4841.

Zoete, V., Cuendet, M.A., Grosdidier, A., and Michielin, O. (2011). SwissParam: a fast force field generation tool for small organic molecules. *J. Comput. Chem.* 32, 2359–2368.

## STAR★METHODS

### KEY RESOURCES TABLE

REAGENT or RESOURCE	SOURCE	IDENTIFIER
<b>Bacterial and virus strains</b>		
<i>S. aureus</i> (ATCC 25923)	Prof. Michael M. Meijler, Ben Gurion University of the Negev, Israel.	N/A
<i>B. subtilis</i> NCIB3610	Prof. Michael M. Meijler, Ben Gurion University of the Negev, Israel.	N/A
<i>E. coli</i>	Prof. Michael M. Meijler, Ben Gurion University of the Negev, Israel.	N/A
<i>P. aeruginosa</i> PAO1	Prof. Michael M. Meijler, Ben Gurion University of the Negev, Israel.	N/A
<b>Biological samples</b>		
Mice blood	Prof. Elena Voronov, Ben Gurion University of the Negev, Israel.	N/A
Mice serum	Prof. Elena Voronov, Ben Gurion University of the Negev, Israel.	N/A
<b>Chemicals, peptides, and recombinant proteins</b>		
CLR01	(Talbiersky et al., 2008)	N/A
CLR03	(Fokkens et al., 2005)	N/A
CLR05	(Dutt et al., 2013)	N/A
PSM $\alpha$ 1 at 98% purity (MGIIAGIIKVIKSLIEQFTGK)	GL Biochem	N/A
PSM $\alpha$ 4 at 98% purity (MAIVGTIIKIIKAIIDIFAK)	GL Biochem	N/A
Brain Heart Infusion Broth	Sigma Aldrich	CAS#53286
Luria broth (Miller)	Sigma Aldrich	CAS#L2542
Hexafluoroisopropanol (HFIP)	Sigma Aldrich	CAS#920-66-1
Trifluoroethanol (TFE)	Sigma Aldrich	CAS#75-89-8
Dimethyl sulfoxide	Sigma Aldrich	CAS#67-68-5
Sodium hydrosulfite	Sigma Aldrich	CAS#7775-14-6
Sodium phosphate monobasic	Sigma Aldrich	CAS#7558-80-7
Thioflavin T	Sigma Aldrich	CAS#2390-54-7
1,2-dioleoyl-sn-glycero-3-phosphoethanolamine (DOPE)	Avanti	CAS#850725
1,2-dioleoyl-sn-glycero-3-phospho-(1'-rac-glycerol) (DOPG)	Avanti	CAS#840475
Cardiolipin	Avanti	CAS#710335
Trimethylammonium-diphenylhexatriene (TMA-DPH)	Thermo Fisher Scientific	CAS#T204
1,2-dimyristoyl-sn-glycero-3-phosphoethanolamine-N-(7-nitro-2-1,3-benzoxadiazol-4-yl) (N-NBD-PE)	Avanti	CAS#810145
1,2-dimyristoyl-sn-glycero-3-phosphoethanolamine-N-(lissamine rhodamine B sulfonyl) (N-Rh-PE)	Avanti	CAS#810157
LIVE/DEAD™ BacLight™ Bacterial Viability Kit	Thermo Fisher Scientific	CAS#L7007
<b>Experimental models: organisms/strains</b>		
C57BL/6 wild type (WT) mice	Harlan Laboratories	

(Continued on next page)

**Continued**

REAGENT or RESOURCE	SOURCE	IDENTIFIER
Software and algorithms		
IMARIS software	Bitplane AG, Zürich, Switzerland	<a href="https://www.imaris.com/products/imiris-for-cell-biologists">imaris.oxinst.com/products/imiris-for-cell-biologists</a>
NAMD 2.13	Theoretical and Computational Biophysics group, University of Illinois at Urbana-Champaign, USA	<a href="https://www.ks.uiuc.edu/Development/Download/download.cgi?PackageName=NAMD">https://www.ks.uiuc.edu/Development/Download/download.cgi?PackageName=NAMD</a>
CLFEP-GUI	Computational Biochemistry, University of Duisburg-Essen, Germany	WEB SERVER: <a href="https://clfep.zmb.uni-due.de/">https://clfep.zmb.uni-due.de/</a>
VMD 1.9.3	Theoretical and Computational Biophysics group, University of Illinois at Urbana-Champaign, USA	<a href="https://www.ks.uiuc.edu/Development/Download/download.cgi?PackageName=VMD">https://www.ks.uiuc.edu/Development/Download/download.cgi?PackageName=VMD</a>
I-TASSER	A Roy, et al. Nature Protocols, 5: 725-738 (2010)	WEB SERVER: <a href="https://zhanglab.ccmb.med.umich.edu/I-TASSER/">https://zhanglab.ccmb.med.umich.edu/I-TASSER/</a>
CorelDraw Graphics Suite	Campus license, University of Duisburg-Essen, Germany	Software link: <a href="https://www.coreldraw.com/de/product/coreldraw/?hp=de2bb1">https://www.coreldraw.com/de/product/coreldraw/?hp=de2bb1</a> Link for university (UDE, Germany) members: <a href="https://www.uni-due.de/zim/services/software/coral-draw">https://www.uni-due.de/zim/services/software/coral-draw</a>

**RESOURCE AVAILABILITY**

**Lead contact**

Further information and requests for resources and reagents should be directed to and will be fulfilled by the lead contact, Gal Bitan ([gbitan@mednet.ucla.edu](mailto:gbitan@mednet.ucla.edu))

**Materials availability**

Reagents generated in this study are available from the Lead Contact with a completed Materials Transfer Agreement.

**Data and code availability**

This study did not generate code.

**EXPERIMENTAL MODEL**

**Ex vivo animal studies**

C57BL/6 wild type (WT) mice were purchased from Harlan Laboratories (Rehovot, Israel). Animal studies were approved and performed according to the guidelines of the Ben-Gurion University of the Negev, Faculty of Health Sciences, Animal Safety Committee (Beer-Sheva, Israel). Female 8- to 10- week-old mice were used in all experiments.

**Bacterial strains and culture media**

*S. aureus* (ATCC 25923) was grown in brain-heart infusion (BHI) broth: 0.5% beef heart, 1.25% calf brains, 0.25% disodium hydrogen phosphate and 0.2% D(+)-glucose. *B. subtilis* NCIB3610, *E. coli* and *P. aeruginosa* PAO1 Seattle were grown in Luria-Bertani (LB) broth: 1% tryptone (Difco), 0.5% yeast extract (Difco) and 0.5% NaCl. When preparing plates, the medium was solidified by the addition of 1% agar. Each strain was grown from a single colony, *B. subtilis* NCIB3610 was grown at 30°C and *S. aureus* (ATCC 25923), *E. coli* and *P. aeruginosa* PAO1 Seattle at 37°C. All the cultures were grown with 220 rpm shaking overnight.

**METHOD DETAILS**

**Peptide preparations**

Lyophilized PSM $\alpha$ 1 or PSM $\alpha$ 4 were dissolved in HFIP at a concentration of 1 mg/mL followed by a 10-min sonication in a bath sonicator at room temperature. HFIP was then evaporated using a mini-rotational vacuum concentrator (Christ, Germany) at 1000 rpm for 2 hr at room temperature. The dried peptide sample was stored at -20°C prior to use. Before using, dried peptide samples were dissolved in 10 mM phosphate buffer, pH 7.4 (Sodium phosphate, dibasic dehydrate, and Sodium phosphate, monobasic monohydrate) to the required final concentration.

### Lipid vesicle preparation

Vesicles consisting of DOPE/DOPG/CL at 0.2:0.55:0.25 or 0.8:0.15:0.05 mole ratio, gram positive and gram negative, respectively, were prepared by dissolving the lipid components in a chloroform/ethanol (1:1, v/v) mixture and drying the solution under vacuum. Small unilamellar vesicles (SUVs) were prepared from the dried lipid powder in 2 mL of 10 mM phosphate buffer, pH 7.4, by sonication, using Sonics Vibra-cell VCX-130 sonicator (Newtown, CT, USA) at room temperature for 10 min at 20% amplitude. Vesicle suspensions were incubated for 1 h at room temperature prior to usage.

### Bacterial growth

Bacterial cultures were grown overnight as described above and then diluted to absorbance density ( $OD_{600}$ ) of 0.05 in fresh medium. The test compounds, CLR01, CLR03 or CLR05 were dissolved in doubly distilled water (DDW) and serially diluted into BHI or LB media in a white, clear bottom, 96-well plate. 50  $\mu$ L of the diluted cells were added to each well. Control wells did not contain molecular tweezers.  $OD_{600}$  values were measured every 20 min for 18 h with continuous shaking at 30°C or 37°C, as appropriate for the different bacteria, using a Microtiter Plate Reader (Varioskan Flash, Thermo). Measurements were performed at a minimum of three biological replicates, each with three technical replicates and results are presented as mean  $\pm$  SD.

### Blood collection

Blood sample was collected under general anesthesia. Topical ophthalmic anesthetic agent is applied to the eye before bleeding and a capillary is inserted into the medial canthus of the eye.

The Blood was collected into anti-coagulant tubes and used in the biofilm assay immediately after collection. To prepare the serum samples, blood was collected into sterile tube and allowed to clot for approximately 30 min and later followed by centrifuge which allowed the serum removal for storing at  $-80^{\circ}\text{C}$  until use.

### Biofilm modulation activity

For static biofilm assays, overnight cultures of *S. aureus* were diluted 1:10 in fresh BHI containing a final concentration of 25 or 50  $\mu\text{M}$  of each molecular tweezer dissolved in DDW or the same volume of DDW as a negative control. Subsequently, the biofilms were grown under non-shaking conditions at 37°C in 96-well plates (Thermo Scientific, Rochester, NY, USA). The cultures were stained using a LIVE/DEAD BacLight Bacterial Viability Kit. After the time incubation (~15min), the stained biofilms were washed twice with PBS. No increase in dead cells was observed in these experiments in the presence of the test compounds, CLR01, CLR03 or CLR05, compared to control biofilm. Biofilm images were taken by CLSM (Plan-Apochromat 20 $\times$ /0.8 M27, Zeiss LSM880, Germany). The collected images were processed using 3D-reconstruction IMARIS software (Bitplane AG, Zürich, Switzerland).

### Biofilm growth in 10% mice serum

100  $\mu\text{L}$  mice serum was added to each well containing overnight cultures of *S. aureus* in fresh BHI (total volume of 1 mL) in the presence or absence of 50  $\mu\text{M}$  of the test compounds, CLR01, CLR03 or CLR05. Biofilms samples were grown under non-shaking conditions at 37°C for 24 hr.

### Biofilm growth in mice blood

995  $\mu\text{L}$  mice blood was added to each well containing overnight cultures of *S. aureus* in fresh BHI (total volume of 1 mL) in the presence or absence of 50  $\mu\text{M}$  of the test compounds, CLR01, CLR03 or CLR05. Biofilms samples were grown under non-shaking conditions at 37°C for 24 h.

### Scanning electron microscopy (SEM)

To assess the effect of 10% mice serum and mice blood on biofilm growth, 24-h *S. aureus* cultures in each medium in the absence or presence of 50  $\mu\text{M}$  molecular tweezers were grown under non-shaking conditions at 37°C as described above. After the time of incubation, the medium was removed and washed several times with PBS buffer. Subsequently, the biofilms were resuspended in PBS buffer and fixed for the SEM experiments. *S. aureus* biofilms were fixed on a poly-L-lysine cover glass, initially using glutaraldehyde 2.5% solution in buffer for 2 h, and then incubated with osmium tetroxide 1% solution, followed by dehydration by rinsing with ethanol/HMDS mixtures. The fixed biofilms were spray coated with a thin gold layer and placed in the microscope for measurements. SEM images were recorded using a JSM-7400 SEM (JEOL LTD, Tokyo, Japan).

### Quantitate biofilm analysis by crystal violet assay

*S. aureus* bacteria were grown on pre-sterilized 96-well flat bottom polystyrene microtiter plates in three biological repeats. The bacteria were diluted to a final  $OD_{600} = 0.05$  and added to the plate in the absence or presence of the desired concentrations of each compound. The plates then were incubated without shaking for 24 h at 37°C. The medium was removed and the biofilm washed with PBS. 200  $\mu\text{L}$  crystal violet (0.1% w/v) were added to each well to stain the biofilms. After 15 min incubation, excess crystal violet was removed and plates were washed and air dried. Finally, the cell-bound crystal violet was dissolved in 30% acetic acid. Biofilm growth was quantified by measuring absorbance at 570 nm using a microplate reader (Varioskan Flash, Thermo). Luminescence values were normalized to the control.

### Thioflavin-T fluorescence fibrillation-kinetics assay

HFIP-treated PSM $\alpha$ 1 was dissolved in DMSO at 10 mM and immediately diluted to 50  $\mu$ M in Tris hydrochloride, pH 7.5, containing filtered ThT diluted from a stock made in ultrapure water. Molecular tweezers were diluted into the reaction mixtures from a 5-mM stock solution made in ultrapure water, as described above, at 1:1 or 1:5 molar ratios. Final concentrations for each reaction were 50  $\mu$ M PSM $\alpha$ 1, 50  $\mu$ M or 25  $\mu$ M molecular tweezer, and 200  $\mu$ M ThT. Blank solutions, not containing the peptide, also were prepared for each reaction. The reaction mixture was placed in black 96-well flat-bottom plates (Greiner bio-one) covered by thermal seal films (EXCEL scientific) and incubated in a plate reader (CLARIOstar BMG LABTECH) at 37°C with 500 rpm shaking for 85 s before each reading cycle monitored every 6 min. A minimum of three biological replicates were performed, each with three technical replicates. Fluorescence was measured by excitation at 438  $\pm$  20 nm and emission at 490  $\pm$  20 nm over a period of 24 h. Triplicate values were averaged, appropriate blanks were subtracted, and the resulting values were plotted against time. The data are presented as mean  $\pm$  SD. Additional experiment was done in the presence of 15  $\mu$ M Lys amino acid.

### Transmission electron microscopy

Samples of PSM $\alpha$ 1 and PSM $\alpha$ 4 in the absence or presence of molecular tweezers were collected from the ThT fibrillation reactions. Five-microliter samples were applied directly onto copper TEM grids with support films of Formvar/Carbon (Ted Pella), which were glow discharged (PELCO easiGlow, Ted Pella) immediately before use. Proteins were allowed to adhere to the grids for 2 min and negatively stained with 5  $\mu$ L of 2% uranyl acetate. Micrographs were recorded using a FEI Tecnai G2 T20 S-Twin transmission electron microscope operated at an accelerating voltage of 200 KeV or a FEI Tecnai G2 T12 TEM operated at an accelerating voltage of 120 kV. Images were recorded digitally by a Gatan US 1000 CCD camera using the Digital Micrograph software.

### Disintegration of mature fibrils

HFIP-treated PSM $\alpha$ 1 aliquots were re-dissolved to 10 mM in 100% DMSO followed by sonication for 10 min in a bath-sonicator and immediately diluted to 1 mM in 10 mM Tris hydrochloride, pH 7.3. The samples were incubated at 37°C with 300-rpm shaking for two days. Subsequently, the samples were diluted to 50  $\mu$ M (monomer concentration), CLR01, CLR03 or CLR05 were added at a 1:1 concentration ratio, and the samples were incubated for 24 h at 37°C. A sample incubated in the absence of molecular tweezers served as a negative control. Samples then were measured by CD spectra or fixed on TEM grids to visualized as described above.

### Fluorescence titration

Fluorescence of the tweezer solutions were measured at  $\lambda_{\text{ex}} = 285$  nm, and the emission spectra were monitored in the range of 300–440 nm using an FL920 spectrofluorimeter (Edinburgh Co., Edinburgh, UK). In a typical titration experiment, 700  $\mu$ L of the host solution (CLR01 or CLR05) was placed in a quartz cuvette, and the PSM $\alpha$ 1 solution was added stepwise (Tables S1 and S2). Emission intensity changes were recorded at 25°C. Change in the intensities of the tweezers' emission bands were calculated by using the following equation:  $(\Delta I_{\text{max}} [\%]) = 100 \bullet (I_0 - I_{\text{max}}) / I_0$ , where  $I_0$  = emission intensity of free tweezers and  $I_{\text{max}}$  = emission intensity of host-guest complexes. Kd values were calculated from the fluorometric titration experiments using a standard nonlinear regression by fitting the columns of host and guest concentration.

### NMR spectroscopy and titration

NMR experiments with CLR01, CLR03, and CLR05 were performed on PSM $\alpha$ 1 to determine the binding site(s) of the tweezer molecules.  $^1\text{H}$ - $^{13}\text{C}$  HSQC spectra were recorded on a 0.77-mM PSM $\alpha$ 1 sample in 200  $\mu$ L D $_2$ O and 200  $\mu$ L trifluoroethanol (TFE) on a Bruker 800 MHz spectrometer equipped with a cryoprobe at 25°C before and after adding CLR01, CLR03, or CLR05 each at 0.1:1, 0.2:1, 0.3:1, and 1:1 molar ratios. The 1:1 ratio is shown in Figure 6.

### Computational details

The initial coordinates of the PSM $\alpha$ 1 peptide were taken from the crystal structure reported with PDB code 5KHB (Towle et al., 2016), in which the formylated methionine was replaced by a methionine. The tweezers-PSM $\alpha$ 1 systems were studied with three production runs of molecular dynamics simulations of 100 ns each.

#### Cluster of peptides as fibril/aggregate model

The structure of the cluster of peptides used as model of the PSM $\alpha$ 1 fibril was constructed based on the crystal structure with PDB ID 6FG4. (Salinas et al., 2018) The model had four layers, for a total of eight peptide fragments (of six amino acids each, including two lysine residues). The PSM $\alpha$ 1 model with eight CLR01/CLR05 tweezers was subjected to three independent replicas of Gaussian accelerated Molecular Dynamics simulations (GaMD) (Pang et al., 2017) for a total sampling of 900 ns for each system (834 ns of production runs after discarding 22 ns of equilibration steps in each replica). Both, MD and GaMD simulations were done with explicit TIP3P water molecules. (Jorgensen et al., 1983) The simulations were performed with 2 fs time step, at a pressure of 1 bar and at a temperature of 300 K. A cut-off of 14 Å was used. The Particle Mesh Ewald method (Darden et al., 1993) was employed for the treatment of long-range electrostatic interactions.

#### PSM $\alpha$ 1 peptide in fibril-like conformation

The disordered structural model of the full-length PSM $\alpha$ 1 peptide (used for the CL-FEP calculations reported in Figure 6G) was built using I-TASSER (Roy et al., 2010; Yang and Zhang, 2015) with the structure with PDB ID 6FG4 (Salinas et al., 2018) as constraint of the amyloidogenic fragment of the peptide. The resulting model was refined with molecular dynamics simulations in explicit water for

50 ns. During this relaxation simulation, harmonic restraints on the amyloidogenic fragment (7-IIKVIK-12) were applied to keep its fibril-like conformation. The first 10 ns of the simulation were discarded in order to ensure the analysis of equilibrated sampling. From there, 4000 conformations of the peptide were obtained and subsequently clustered using a backbone RMSD cutoff of 8 Å (the rather large cutoff value obeys to the disordered nature of the peptide). The largest cluster of conformations comprised 51.3% of the sampled trajectory frames. Consequently, the structure in its center was selected as representative of the disordered conformation of PSM $\alpha$ 1.

For the binding energy calculations, the Central Limit Free Energy Perturbation (CL-FEP) method was used and the convergence of the values was assessed (Tables S5–S7). (Ruiz-Blanco and Sanchez-Garcia, 2020)

All simulations were performed using NAMD2.13 (Phillips et al., 2005, 2020) and the CHARMM36m force field (Kluda et al., 2010; Vanommeslaeghe and MacKerell, 2015). For the tweezers a set of parameters obtained with the Swissparam server (Zoete et al., 2011) and extensively tested by us (Bier et al., 2013; Dutt et al., 2013; Lump et al., 2015; Trusch et al., 2016) was used. VMD 1.9.3 (Humphrey et al., 1996) was employed for the analysis and visualization of the trajectories.

### Fluorescence anisotropy

The fluorescence probe TMA-DPH was incorporated into the SUVs (DOPE/DOPG/CL or DOPE/DOPG/CL 0.2:0.55:0.25 and 0.8:0.15:0.05 mole ratio, respectively) by adding the dye dissolved in THF (1 mM) to vesicles up to a final concentration of 1.25  $\mu$ M. The prepared solutions contained 30  $\mu$ L vesicles in the presence or absence of different tweezer concentration were mix in a quartz cuvette (path length 10 mm) and the remaining volume was fill up to a total of 1 mL with 10 mM phosphate buffer, pH 7.4. After 30 min of incubation at 30°C of TMA- DPH, fluorescence anisotropy was measured at  $\lambda_{ex}$  = 360 nm and  $\lambda_{em}$  = 430 nm using an FL920 spectrofluorimeter (Edinburgh Co.). Data were collected before and after the addition of the tested compounds (CLR01, CLR05 or CLR03). Anisotropy values were automatically calculated by the spectrofluorimeter software using the equation:  $r = (I_{VV} - G I_{VH}) / (I_{VV} + 2G I_{VH})$ ,  $G = I_{HV} / I_{HH}$ , in which  $I_{VV}$  is with excitation and emission polarizers mounted vertically,  $I_{HH}$  corresponds to the excitation and emission polarizers mounted horizontally,  $I_{HV}$  is the excitation polarizer horizontal and the emission polarizer vertical, and  $I_{VH}$  requires the excitation polarizer vertical and emission polarizer horizontal. Each experiment was repeated at least three times. Results are presented as mean  $\pm$  SD of ten replicates.

### Förster resonance energy transfer (FRET)

SUVs (DOPE/DOPG/CL 0.2:0.55:0.25 mole ratio) were prepared by dissolving the lipid components in chloroform/ethanol and drying together under vacuum, followed by dissolution in phosphate buffer, pH 7.4, and sonication of the aqueous lipid mixture at room temperature for 10 min using a probe-sonication. Prior to drying, the lipid vesicles were supplemented with N-NBD-PE and N-Rh-PE at a 500:1:1 molar ratio (phospholipid:N-NBD-PE:N-Rh-PE). The prepared solutions contained 30  $\mu$ L vesicles in the presence or absence of different tweezer concentration were mix in a quartz cuvette (path length 10 mm) and the remaining volume was fill up to a total of 1 mL with 10 mM phosphate buffer, pH 7.4. Fluorescence emission spectra were acquired at different tweezers concentrations ( $\lambda_{ex}$  = 469 nm) in the range of 490–650 nm using an FL920 spectrofluorimeter (Edinburgh Co., Edinburgh, UK). The Fd/Fa ratio was calculated as a direct measure of FRET between the N-NBD-PE donor and N-Rh-PE acceptor [Fd and Fa represent the fluorescence intensity of the donor (536 nm) and acceptor (591 nm), respectively]. For reference, the Fd/Fa ratio of a blank measurement (vesicles only, prior to addition of tested compounds) was calculated and used as a normalizing constant. The data are representative of three independently performed experiments and are presented as mean  $\pm$  SD.

### CD spectroscopy

CD spectra was recorded at  $t = 0$  and  $t = 24$  hr in the range of 190–260 nm at room temperature on a Jasco J-715 spectropolarimeter, using 1-mm quartz cuvettes. The prepared solutions had a total volume of 300  $\mu$ L and contained 50  $\mu$ M PSM $\alpha$ 1 or PSM $\alpha$ 4 dissolved in 0.1% acetonitrile in deionized water, in the absence or presence of 50  $\mu$ M CLR01, CLR05 or CLR03. CD signals resulting from tweezers and buffer were subtracted from the corresponding spectra. The measured ellipticity was normalized according to path-length, sample concentration and number of residues.

### QUANTIFICATION AND STATISTICAL ANALYSIS

In general, data were analyzed in Excel and presented as mean  $\pm$  SD. Details of replicates and data analysis for each experiment can be found in the figure legends or methods section.